Atmos. Chem. Phys., 19, 15073–15086, 2019
https://doi.org/10.5194/acp-19-15073-2019

Atmospheric Chemistry and Physics
Open Access
EGU

Effect of NO_x on 1,3,5-trimethylbenzene (TMB) oxidation product distribution and particle formation

Epameinondas Tsiligiannis[1], Julia Hammes[1], Christian Mark Salvador[1], Thomas F. Mentel[1,2], and Mattias Hallquist[1]

[1]Department of Chemistry and Molecular Biology, University of Gothenburg, Gothenburg, Sweden
[2]Institute of Energy and Climate Research, Troposphere (IEK-8), Forschungszentrum Jülich GmbH, Jülich, Germany

Correspondence: Mattias Hallquist (hallq@chem.gu.se)

Received: 25 April 2019 – Discussion started: 17 May 2019
Revised: 23 October 2019 – Accepted: 8 November 2019 – Published: 13 December 2019

Abstract. Secondary organic aerosol (SOA) represents a significant fraction of the tropospheric aerosol and its precursors are volatile organic compounds (VOCs). Anthropogenic VOCs (AVOC) dominate the VOC budget in many urban areas with 1,3,5-trimethylbenzene (TMB) being among the most reactive aromatic AVOCs. TMB formed highly oxygenated organic molecules (HOMs) in an NO_x-free environment, which could contribute to new particle formation (NPF) depending on oxidation conditions where elevated OH oxidation enhanced particle formation. The experiments were performed in an oxidation flow reactor, the Go:PAM unit, under controlled OH oxidation conditions. By addition of NO_x to the system we investigated the effect of NO_x on particle formation and on the product distribution. We show that the formation of HOMs, and especially HOM accretion products, strongly varies with NO_x conditions. We observe a suppression of HOM and particle formation with increasing NO_x/ΔTMB ratio and an increase in the formation of organonitrates (ONs) mostly at the expense of HOM accretion products. We propose reaction mechanisms and pathways that explain the formation and observed product distributions with respect to oxidation conditions. We hypothesise that, based on our findings from TMB oxidation studies, aromatic AVOCs may not contribute significantly to NPF under typical NO_x/AVOC conditions found in urban atmospheres.

1 Introduction

Volatile organic compounds (VOCs) are ubiquitous in the atmosphere and major precursors for secondary organic aerosol (SOA). SOA represents a dominant fraction of the tropospheric aerosol (Hallquist et al., 2009; Shrivastava et al., 2017; Gentner et al., 2017) and affects climate (Intergovernmental Panel on Climate, 2014) and health (WHO, 2016). Consequently research interest in SOA formation and properties ranges from remote atmospheres (Ehn et al., 2012, 2014; Kristensen et al., 2016) to densely populated and polluted environments (Chan and Yao, 2008; Hu et al., 2015; Guo et al., 2014; Hallquist et al., 2016). Following the study by Ehn et al. (2012), highly oxygenated organic molecules (HOMs) with low volatilities, formed from the oxidation of biogenic volatile organic compounds (BVOCs), have attracted much research interest (Crounse et al., 2013; Ehn et al., 2014; Jokinen et al., 2014, 2015; Mentel et al., 2015; Yan et al., 2016; Berndt et al., 2016; Bianchi et al., 2019). These compounds have been shown to contribute to new particle formation (NPF) and to SOA growth (Ehn et al., 2014; Bianchi et al., 2016; Kirkby et al., 2016; Trostl et al., 2016; McFiggans et al., 2019), making them an important factor in the formation of atmospheric SOA. These oxidation products can be either described as HOM based on their high oxygen number ($O > 6$) (Bianchi et al., 2019) or as extremely low volatility organic compounds (ELVOCs) based on their volatility (Donahue et al., 2012; Trostl et al., 2016). In this study, we will refer to oxidation products as HOMs, because not all of the measured compounds may fulfill the criteria for ELVOCs (Trostl et al., 2016; Kurtén et al., 2016). Gas-phase autoxidation of alkylperoxy radicals (RO_2) has been

proposed as the formation mechanism for HOMs (Crounse et al., 2013; Ehn et al., 2014; Jokinen et al., 2014). After the initial reaction of an oxidant with the VOC and subsequent addition of O_2 to the alkyl radical (R), the produced RO_2 isomerises via intra-molecular H abstraction (H shift). During this process a hydroperoxide group and a new R are formed. Additional O_2 addition and H-shift sequences can introduce large amounts of oxygen to the molecule and subsequently lower the vapour pressure. The chemistry of aromatic compounds is somewhat different compared to other VOCs as they can lose their aromaticity during the initial OH attack while retaining their ring structure. Moreover, reaction products are more reactive than the parent compound. The produced RO_2 species form an oxygen bridge, a bicyclic and potentially tricyclic alkyl radical (Molteni et al., 2018; Wang et al., 2017), before further oxidation processes open the ring structure. For 1,3,5-trimethylbenzene (TMB), emitted from combustion sources in the urban environment, Molteni et al. (2018) proposed a generalised reaction scheme for HOM formation after OH addition. According to their scheme, first-generation alkylperoxy radicals with the general formula of $C_9H_{13}O_{5-11}$ were formed from the initial OH attack and subsequent H-shift and O_2 addition sequences. A postulated second OH attack would result in propagating peroxy radical chains, yielding radicals with the general formula $C_9H_{15}O_{7-11}$.

Generally, the termination reaction of RO_2 (with a general $m/z = x$) with HO_2 leads to the formation of hydroperoxides ($m/z = x + 1$), while termination reactions with other RO_2 species can lead to the formation of a carbonyl ($m/z = x - 17$), a hydroxy group ($m/z = x - 15$) or dimers ($m/z = 2x - 32$) (Mentel et al., 2015; Jokinen et al., 2014; Rissanen et al., 2014). The propagation reaction of RO_2 with another RO_2 or NO also results in the formation of RO ($m/z = x - 16$). The RO can undergo internal H shift leading to the formation of a hydroxy group and subsequently a new peroxy radical, which can continue the autoxidation sequences. The alkoxy step shift of the observed m/z by 16 leads to an overlap of different termination product sequences. During extensive oxidation the first-generation products are subject to secondary chemistry, increasing the numbers of products. Molteni et al. (2018) found several closed-shell monomer products with the general formula $C_9H_{12-16}O_{5-11}$ from the oxidation of TMB with OH. The formation of dimers with different numbers of H atoms in their study was explained by reactions of two first-generation RO_2 radicals ($C_{18}H_{26}O_{5-10}$): one first- and one second-generation RO_2 ($C_{18}H_{28}O_{9-12}$) or two second-generation RO_2 species resulting in the dimer $C_{18}H_{30}O_{11}$. Although dimers have in general lower O : C ratios than monomers, they are expected to be less volatile due to higher molecular weight and more functional groups, making them candidates to participate in nucleation processes (Kirkby et al., 2016).

Organonitrates (ONs) are formed as soon as sufficient NO_x is present in the atmosphere. ONs are highly important for the reactive nitrogen budget wherein the formation of highly functionalised organic nitrates can contribute significantly to secondary organic aerosol (Lee et al., 2016; Bianchi et al., 2017). In this study we refer to compounds that only consist of H, C and O as HOM monomers or HOM dimers and to N-containing compounds as ONs.

NO_x influences the oxidation of organics directly by changing oxidant levels (reducing or increasing OH, depending on the NO_x regime) and indirectly by influencing RO_2 chemistry. In high NO_x environments such as urban areas, the reaction of NO with RO_2 radicals can compete with the autoxidation mechanism (Reactions R1 and R2) and thus potentially inhibit HOM while favouring some ON formation (Reaction R1 with a yield of up to 0.3).

$$RO_2 + NO \rightarrow RONO_2, \quad \text{(R1)}$$

$$\rightarrow RO + NO_2. \quad \text{(R2)}$$

Although ONs may have high O : C ratios, they differ from HOMs as they contain at least one nitrogen atom. While HOM formation from BVOCs has been intensively studied, only few studies have been conducted focusing on the formation of HOMs from aromatic anthropogenic volatile organic compounds (AVOCs) (Molteni et al., 2018; Wang et al., 2017). However, these studies indicate that AVOCs have a strong potential to form HOMs under NO_x-free conditions and proposed that they may play a crucial role in NPF and particle growth of SOA in urban areas. Regarding SOA yields, a number of smog chamber studies have been conducted in order to investigate the oxidation of TMB with OH radicals under different NO_x and aerosol seed conditions (Paulsen et al., 2005; Rodigast et al., 2017; Wyche et al., 2009; Huang et al., 2015; Sato et al., 2012). They reported that under higher NO_x : VOC conditions, SOA yield is reduced compared to medium or lower NO_x : VOC conditions. The NO_x : VOC ratio, in almost all studies, was < 1, apart from one experiment (Wyche et al., 2009), with NO_x : VOC $= 1.9$ in which the SOA yield was 0.29, compared to yields of up to 7.47 under lower NO_x conditions.

In this study we investigate the oxidation of TMB in a laminar-flow reactor, while different NO_x and OH conditions were applied. A nitrate chemical ionisation atmospheric pressure interface time-of-flight mass spectrometer (CI-APi-TOF-MS) (Junninen et al., 2010; Jokinen et al., 2012) was used to monitor the oxidation product distribution. We show the formation of HOMs and nitrate-containing compounds with and without NO_x added to the reaction system. Possible mechanisms leading to the formation of ONs and suppression of particle formation are discussed.

2 Materials and methods

The measured HOMs were generated using the laminar-flow Gothenburg potential aerosol mass reactor (Go:PAM), initially described by Watne et al. (2018). The Go:PAM is a

100 cm long and 9.6 cm wide quartz glass cylinder which is irradiated over a length of 84 cm by two 30 W Phillips TUV lamps (254 nm); a schematic is shown in Fig. 1. The OH radicals are produced inside Go:PAM by photolysing O_3 in the presence of water vapour. The O_3 is generated outside Go:PAM by photolysing pure O_2 (UVP Pen-Ray® mercury lamps, 185 nm) and distributed in 3 L min^{-1} particle-free and humidified air (Milli-Q) over the reactor cross section. The VOC was introduced through a gravimetrically characterised diffusion source (see Fig. S2) centrally at the top of the reactor with a flow of 8 L min^{-1} while NO was introduced via a NO gas cylinder. Flows were adjusted for a median residence time of 34 s in Go:PAM. A funnel-shaped device is subsampling the central part of the laminar flow to minimise wall effects on the sample. A condensation particle counter (CPC, 3775 TSI) was used to measure the number particle concentration in the sample flow. O_3 was monitored by a model 202 monitor (2B Technologies), relative humidity by a Vaisala HMP60 probe and NO_x by a model 42i monitor (Thermo Scientific) over the course of the experiments. The OH exposure, over the residence time in the reactor, for NO_x-free conditions without added TMB, was measured using SO_2 titration (Teledyne T100) as described by Kang et al. (2007). Gas-phase oxidation products were measured with an atmospheric pressure interface high-resolution time-of-flight mass spectrometer (APi-TOF-MS, Aerodyne Research Inc. and Tofwerk AG) (Junninen et al., 2010; Jokinen et al., 2012) in connection with a A70 CI-inlet (Airmodus Ltd) (Eisele and Tanner, 1993). The CI inlet is a laminar-flow inlet operated with a sheath flow of 20 L min^{-1} containing NO_3^- ions that are generated by ionising HNO_3 using an ^{241}Am foil upstream in the inlet design. The sample stream from Go:PAM is introduced in the centre of the sheath flow at a rate of 8 L min^{-1}. The NO_3^- ions are electrostatically pushed into the sample flow and form stable adducts with sample molecules as described by Ehn et al. (2012). The reaction time of oxidation products and NO_3^- is a few hundred milliseconds before being subsampled into the TOF-MS at 0.8 L min^{-1} by a critical orifice. Differential pumping decreased the pressure from 103 mbar in the CI source to 10^{-6} mbar in the TOF extraction region, where HOMs are detected as negatively charged clusters with NO_3^-.

A kinetic box model was used to simulate the chemistry in the Go:PAM reactor. The core of the model was first described by Watne et al. (2018). The model consists of 32 species and 68 reactions now including TMB chemistry partly from the MCM v3.3.1 (Jenkin et al., 2003) as well as proposed mechanisms and rate coefficients for NO_2 chemistry (Atkinson et al., 1992; Finlayson-Pitts and Pitts, 2000) and highly oxygenated compounds (Ehn et al., 2014; Berndt et al., 2018; Zhao et al., 2018) (see Table S2). The photon flux used in the simulations was tuned to match measured decay of O_3, and an OH sink was added to match the observed OH exposure in the background experiment, i.e. without the addition of TMB. The model was run for all experiments with and without NO_x. Primarily, the modelled output on OH exposure for each experiments was used to interpret the results and for calculating the consumed TMB. However, generally the modelling output was also used to understand the effects of changing experimental conditions on monomer, dimer and organonitrate (ON) production. The experiments without NO_x were named 1–4, denoting the increase in OH exposure, and experiments with NO_x were denoted according to their NO_x/ΔTMB ratio and high (H) or low (L) OH exposure as seen in Table 1.

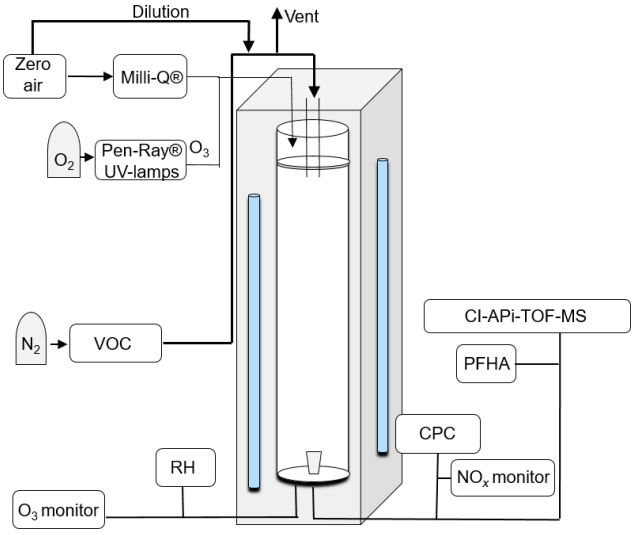

Figure 1. Schematic of the experimental setup with the Go:PAM chamber connected to the CI-APi-TOF-MS.

3 Results and discussions

Table 1 summarises eight experiments where TMB has been oxidised by various amounts of OH using the Go:PAM unit. Generally, a high OH production, induced either by increased light exposure (two lamps) or elevated ozone concentration, resulted in new particles (e.g. experiments 3 and 4), while addition of NO_x reduced or suppressed the particle formation. The results from the kinetic model show that the amount of reacted TMB ranges from 5 to 30 ppb, depending on OH exposure (Fig. S1 in the Supplement). An overview of the oxidation product distribution measured with the CI-APi-TOF-MS for different conditions is shown in Figs. 3 and 4. The compounds were detected as nitrate clusters at $m/z = \text{mass}_{\text{compound}} + 62$. The spectra in Figs. 3 and 4 show significant ion signals from oxygenated hydrocarbons retaining the nine carbons from the original TMB with either even H numbers (closed shell) or odd H numbers (open shell) with a limited number of products from fragmentation, i.e. ions with less than nine carbon atoms. C_9 compounds with an O/C ratio of 6/9 or higher were classified as HOM monomers with the general formula $C_9H_{12-16}O_{6-11}$

Table 1. Experimental conditions for experiments with 30 ppb TMB. Ozone and initial NO_x concentration at time zero are given in parts per billion (ppb) and explicitly modelled OH exposure in number of molecules second per cubic centimetre (molec s cm^{-3}). TMB reacted (ΔTMB) in parts per billion (ppb) after a reaction time of 34 s and particle number concentration given in no. cm^{-3} after reaching steady state in the Go:PAM. RH in all experiments was 38 %.

Experiment	$[O_3]_0$	$[NO_x]_0$	OH exposure	ΔTMB	NO_x / ΔTMB	Particle number	Contribution of top-10 species (%)
1	~ 19	5	3.5×10^9	5.4	0.9	–	28.6
2	~ 19	5	7.1×10^9	9.9	0.5	–	29.8
3	~ 100	3	3.8×10^{10}	26	0.1	60 ± 14	38.6
4	~ 100	3	2.1×10^{11}	30	0.1	1610 ± 217	35.9
NOx9	~ 9	82	6.3×10^9	9	9.1	–	52.4
$NOx3_L$	~ 12	38	7.9×10^9	11	3.5	–	42.3
$NOx3_H$	~ 100	79	3.1×10^{10}	25	3.2	–	34.2
NOx1	~ 100	35	9.1×10^{10}	30	1.2	170 ± 50	30.5

in the mass m/z range 280–360. Oxygenated hydrocarbons found in the m/z range 460–560 containing ^{18}C were classified as dimers with chemical formulas $C_{18}H_{24-30}O_{10-16}$. The monomer with the highest intensity detected was $C_9H_{14}O_7$, m/z 296. The highest intensities among the dimers were $C_{18}H_{26}O_{10}$, $C_{18}H_{28}O_{11}$ and $C18H_{28}O_{12}$ at m/z 464, m/z 482 and m/z 498, respectively. In addition to HOM monomers and dimers, nitrogen-containing compounds were found as C_9 compounds with one or two N or C_{18} compounds with one N. The nitrogen-containing compounds were of the general formulas $C_9H_{12-18}NO_{6-13}$, $C_9H_{12-18}N_2O_{8-15}$ and $C_{18}H_{18-24}NO_{6-10}$. The dominating ONs were $C_9H_{13}NO_8$ at m/z 325, $C_9H_{15}NO_{10}$ at m/z 359 and $C_9H_{14}N_2O_{10}$ at m/z 372. In the experiments where NO_x was added, the formation of ON compounds was increasing with the NO_x concentration. In parallel, the levels of HOM monomers and dimers were reduced with NO_x concentration, where dimers were affected stronger than monomers. Even if the fragmentation products were limited some fragmentation leading to less than nine carbons could be observed. The most prominent fragments were assigned molecular formulas $C_4H_7NO_7$ at m/z 243, $C_4H_6O_{12}$ at m/z 246, $C_5H_6O_{12}$ at m/z 258 and $C_6H_9NO_7$ at m/z 269. Some compounds with C numbers of 15 and 17 were detected in the m/z range 270–560, but their contribution to the total signal was negligible (Fig. 3).

The relative contributions of the different compound classes to the total assigned signal are shown in Fig. 2. It is apparent that HOM monomers and dimers dominate the experiments with low NO_x. The contribution of the monomers to the total oxidation product signal ranges from 20.7 %–42.1 % and dimers make 6.8 %–43.3 % of the total signal, depending on experimental conditions. Dimer contributions are highest at high OH exposure (experiments 3 and 4 with estimated OH exposures of 3.8×10^{10} and 2.1×10^{11} molec s cm^{-3}, respectively) and decrease with increasing NO_x. Nitrated compounds dominated the spectra with contributions of up to ~ 75 % in the experiments with the highest amount of NO_x. Surprisingly, some nitrated compounds were also found in the experiments without added NO_x, which may stem from background NO contamination ($\sim$ 3–5 ppb).

Recently, Molteni et al. (2018) assigned 17 compounds making up 80 % of the total detected signal for HOM oxidation products from the reaction of TMB with OH. Their compound with the highest fraction of the signal (24.2 %) was the dimer $C_{18}H_{26}O_8$. This compound was not detected in our study. We did not detected deprotonated compounds in the mass m/z range 270–560, HOM monomers with 17 H atoms, nor compounds with O/C < 0.55 which were found by Molteni et al. (2018). However, we did find 10 of the previously reported 17 monomers and dimers in our spectra. The oxidation product distributions in our experiments are in general term more diverse, i.e. we found more compounds with smaller yields compared to Molteni et al. (2018). In our experiments the highest 20 compounds together explain 46 %–63 % of the total signal with the individual highest oxidation products contributing only between 4.4 % and 16 %. These differences can be the result of different experimental conditions and setup. In our study the residence time is almost double compared to Molteni et al. (2018), leading to the formation of more oxidised compounds, especially more oxidised dimers, which have been reported in this study. In addition we produce OH radicals through irradiation at 254 nm in the full length of the flow reactor, enhancing the effects of secondary chemistry. Despite these differences there is a general agreement on the conclusions for the NO_x-free conditions with the Molteni et al. (2018) study where one rapidly forms HOMs of very low volatility, which can initiate NPF.

The amount of TMB reacted after 34 s in the experiments ranges from 30 ppb (almost all) in experiment 4 to 5 ppb in experiments 1 and NOx9 (compare Table 1 and Fig. S1). The signal intensities of the HOM monomers are increas-

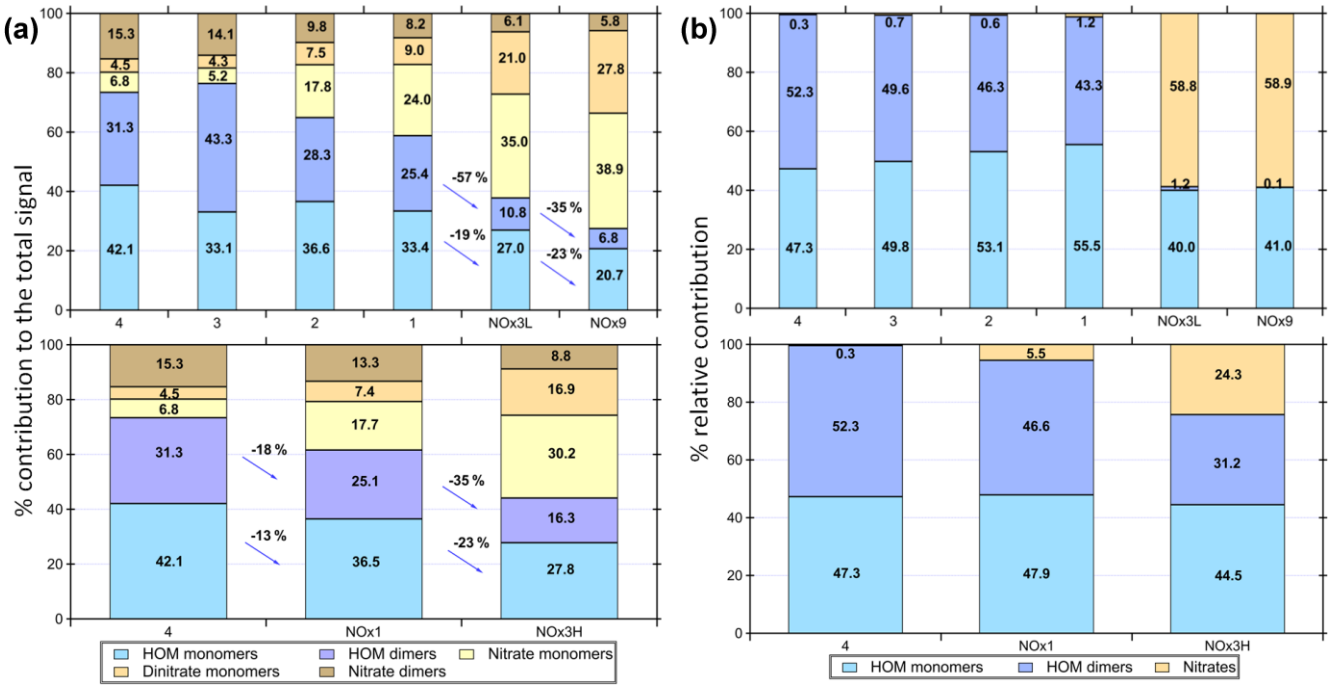

Figure 2. **(a)** Overview of different compound groups to the total explained signal. Top panel illustrates the influence of a decrease in OH exposure (experiments 4–1) and further decrease after adding NO_x in experiments NOx3L and NOx9. Dimers show a larger relative reduction than monomers with increasing NO_x/VOC ratio. Bottom panel shows the influence of increased NO_x/VOC ratio on the product distribution. Experiments 4, 3 and NOx1 resulted in particle formation. **(b)** Modelled product distribution shown as lumped categories of nitrated compounds, HOM monomers and dimers and their relative contributions.

ing with increasing OH exposure. Dimer compounds also increase with increasing OH and reach their highest levels in experiment 3, resulting in the highest ratio of dimer to monomer (see Fig. 2). Faster conversion of TMB will result in higher initial RO_2 levels enabling faster $RO_2 + RO_2$ (self-)reaction. The concentration profile of RO_2 in experiments 1 and 2 is lower and more evenly spread out over the length of the Go:PAM (Fig. S1), and the influence of the $RO_2 + RO_2$ reaction will be less in these experiments compared to experiments 3 and 4. Enhanced OH exposure does not only affect the monomer/dimer ratio but also the total amount of compounds measured. Observed compounds were 10 times higher in the high OH exposure experiments 3 and 4 compared to experiments 1 and 2. This was also valid for the experiments with added NO_x (NOx1 and $NOx3_H$ vs. $NOx3_L$ and NOx9). Under high OH exposure (experiment 4) the major HOM monomer is $C_9H_{14}O_7$ with a contribution of 5.5 % to the total explained signal, followed by $C_9H_{16}O_9$ and $C_9H_{14}O_8$, contributing 4.6 % and 4.5 %, respectively.

At the lowest OH exposure (experiment 1) the major signals comprise the monomer $C_9H_{12}O_{10}$ and the dimers $C_{18}H_{26}O_{10}$ and $C_{18}H_{28}O_{11}$, contributing 4.4 %, 4.0 % and 3.4 % to the total, respectively. These dimer compounds, $C_{18}H_{26}O_{10}$ and $C_{18}H_{28}O_{11}$, are the highest signals in experiments 2 and 3. Two open-shell species were found among the larger signals in experiments 1 and 2 (see Fig. 3): $C_9H_{15}O_8$ and $C_9H_{15}O_7$.

The number of H atoms is a characteristic for HOM monomers and dimers. An overview of different oxidation product generations is given in Table 2. We observe HOM monomers with 12–16 H atoms and all compounds with an even number of H are closed-shell products. Compounds with an uneven number of H atom changes. are open-shell molecules (radicals). Following the proposed termination scheme by Mentel et al. (2015), compounds with 12 H atoms can be identified as first-generation monomers (terminated from $C_9H_{13}O_x$ radicals, Reaction R3) and compounds with 16 H atoms as second-generation monomers (terminated from $C_9H_{15}O_x$ radicals, Reaction R4). $C_9H_{14}O_x$ can be either first- or second-generation products and originate from either $C_9H_{13}O_x$ or $C_9H_{15}O_x$ (Reactions R5 and R6).

$$C_9H_{13}O_x + RO_2 \rightarrow C_9H_{12}O_{x-1} + ROH + O_2, \quad \text{(R3)}$$

$$C_9H_{15}O_x + RO_2 \rightarrow C_9H_{16}O_{x-1} + R'CHO + O_2, \quad \text{(R4)}$$

$$C_9H_{13}O_{x+1} + RO_2 \rightarrow C_9H_{14}O_x + R'CHO + O_2, \quad \text{(R5)}$$

$$C_9H_{15}O_{x+1} + RO_2 \rightarrow C_9H_{14}O_x + ROH + O_2. \quad \text{(R6)}$$

The RO_2 radicals, $C_9H_{13,15}O_x$, can form dimers likely via the reaction

$$\text{HOM-RO}_2 + \text{HOM-RO}_2 \rightarrow \text{HOM-DIMER} + O_2. \quad \text{(R7)}$$

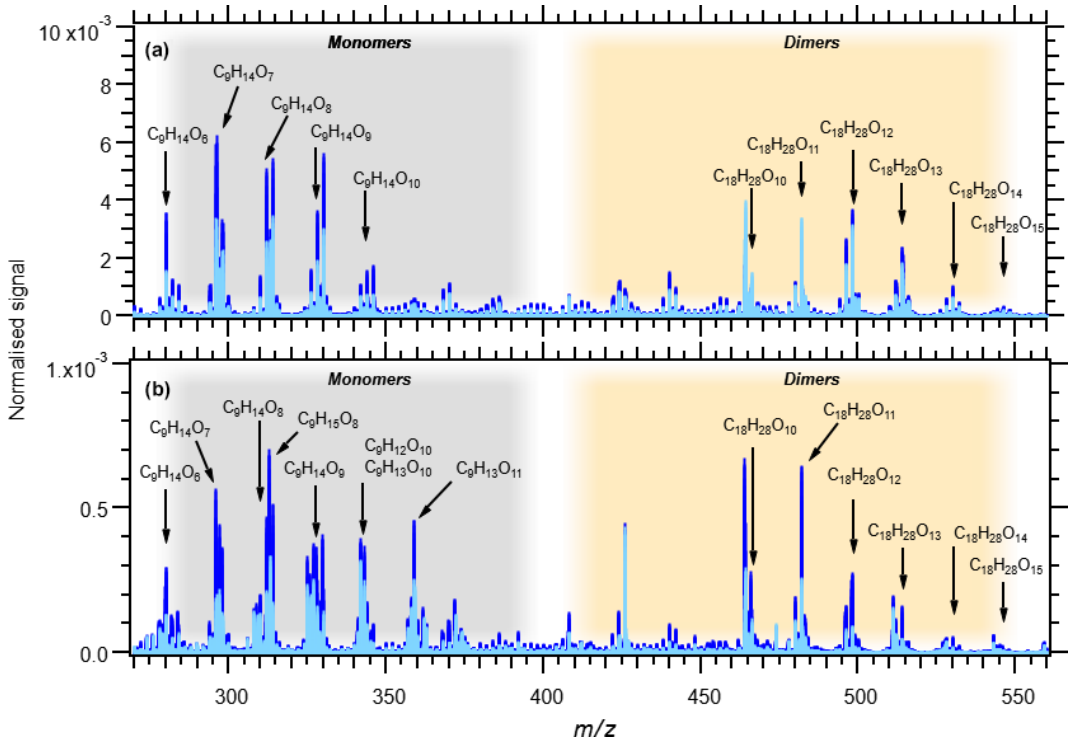

Figure 3. Mass spectra of all experiments without NO_x: 1–4. Panel **(a)** shows experiments 3 (light blue) and 4 (blue) with OH exposure of 2.87×10^{11} and 3.47×10^{11} molec s cm^{-3}, respectively. Panel **(b)** shows experiments 1 (light blue) and 2 (blue) with OH exposure of 3.47×10^{10} and 7.62×10^{10} molec s cm^{-3}, respectively. The signal at m/z 426 is associated with the mass calibration using perfluoroheptanoic acid (PFHA). Note the 10 times lower normalised signal scale in **(b)**.

Table 2. Contribution of oxidation product families to the total signal between m/z 270 and 560.

Compound family	1	2	3	4	NOx9	$NOx3_L$	$NOx3_H$	NOx1
$C_9H_{12}O_x$	11.3	7.8	3.5	5.4	8.5	9.3	5.9	5.4
$C_9H_{13}O_x$	5.7	4.5	3.3	2.1	6.0	7.0	5.6	4.2
$C_9H_{14}O_x$	8.3	10.8	9.9	17.4	4.3	6.6	8.0	13.0
$C_9H_{15}O_x$	5.6	7.2	9.4	4.1	2.4	3.3	4.6	4.7
$C_9H_{16}O_x$	4.8	8.0	7.7	14.5	1.5	2.5	4.8	10.3
$C_{18}H_{26}O_x$	8.5	9.1	8.5	9.3	0.8	2.0	2.7	6.0
$C_{18}H_{28}O_x$	7.1	9.9	9.3	11.0	0.4	1.2	2.6	6.9
$C_{18}H_{30}O_x$	0.7	1.0	2.3	2.6	0.4	0.4	0.9	1.7
$C_9H_{13}NO_x$	6.2	4.7	0.6	0.6	26.8	17.1	10.1	4.8
$C_9H_{15}NO_x$	6.4	5.6	0.7	0.9	3.7	10.3	14.5	8.5
$C_9H_{14}N_2O_x$	2.1	1.7	1.0	1.1	18.7	11.8	7.5	1.9

Such a reaction is possible between any HOM-RO_2 first- or second-generation (and other C_9 peroxy radicals with sufficient high abundance). Two first-generation HOM-RO_2 species will result in $C_{18}H_{26}O_x$ dimers (Reaction R8), while one first- and one second-generation HOM-RO_2 produce a $C_{18}H_{28}O_x$ (Reaction R9) and dimerisation of two second-generation HOM-RO_2 species will result in dimers of the formula $C_{18}H_{30}O_x$ (Reaction R10).

$$C_9H_{13}O_x + C_9H_{13}O_x \rightarrow C_{18}H_{26}O_{x-2} + O_2, \quad \text{(R8)}$$

$$C_9H_{13}O_x + C_9H_{15}O_x \rightarrow C_{18}H_{28}O_{x-2} + O_2, \quad \text{(R9)}$$

$$C_9H_{15}O_x + C_9H_{15}O_x \rightarrow C_{18}H_{30}O_{x-2} + O_2. \quad \text{(R10)}$$

A closer examination of the contribution of different HOM generations in Table 2 shows that first-generation monomers with 12 H atoms are showing the highest contribution in experiments with low OH exposure (experiments 1, 2), while

monomers with 14 H atoms gain importance with higher OH exposure. The second-generation monomers with 16 H atoms dominate in experiments with the highest OH exposure (experiments 3, 4). The dimer population with 28 H atoms has a larger fraction of the total signal at higher OH exposures compared to dimers with 26 H atoms. Dimer population with 30 H atoms is generally lower than other dimers but has the highest fraction in experiment 4. The overall dimer fraction of up to 43 % in this study (Fig. 2) is similar to the dimer fraction of 40 % reported by Molteni et al. (2018). However, the relative contributions of monomer and dimer generations differ. We find higher contributions of H_{12} monomers (up to 11 %) and a higher contribution of H_{28} dimer (up to 12 %) under our experimental conditions. The contribution of H_{14} monomers and H_{26} dimers is significantly less compared to that reported in Molteni et al. (2018).

Increasing OH exposure promotes second OH attacks on oxidation products leading to the observed reduction of first-generation products ($C_9H_{12}O_x$) as well as an increase in second-generation products ($C_9H_{14}O_x$ and $C_9H_{16}O_x$). The $C_9H_{14}O_x$ products have mainly characteristics of second-generation products, as their contribution is enhanced in the experiments with higher OH exposures (Table S1 in the Supplement), in which there is an enhanced possibility for secondary chemistry initiated by reaction of OH with the first-generation products. The increased oxidation degree can also explain the formation of dimers ($C_{18}H_{28}O_x$) from first- and second-generation RO_2 ($C_9H_{13}O_x$ and $C_9H_{15}O_x$) at higher OH exposure and the increase in second-generation dimers. Open-shell species are observed as first-generation RO_2 ($C_9H_{13}O_x$) and have a higher contribution at lower OH exposures. Second-generation RO_2 species ($C_9H_{15}O_x$) have the highest contribution in experiment 3. At the highest OH exposures in experiment 4, the contribution of $C_9H_{15}O_x$ radicals, one of the top-10 contributors to the signal (Table S1), is reduced, while the contribution of the second-generation products ($C_9H_{14}O_x$ and $C_9H_{16}O_x$) and dimers increased.

In this study the contribution of $C_{18}H_{28}O_x$ shows that both first- and second-generation HOM-RO_2 species were dimerising. The kinetics of dimer formation, if produced from RO_2 self-reaction, depends on the square of [HOM-RO_2] and their relative importance will increase with the RO_2 concentration. Increased local RO_2 concentrations (in the first part of the Go:PAM) would explain the increase of dimers with increasing OH exposure.

Substantial particle formation was observed in experiment 4, under the highest OH exposure. Although the amount of reacted TMB in experiments 3 and 4 is similar (26 and 30 ppb, respectively), significant particle formation was not observed under the conditions of experiment 3. The rate at which new particle formation (nucleation) occurs is related to the chemical composition and concentration of the nucleating species (McGraw and Zhang, 2008). After reaching the critical nucleus, particle growth becomes spontaneous in the presence of condensable vapour. Apparently, the local concentration of nucleating species or condensable vapour was not high enough in experiment 3 to yield large numbers of particles, compared to experiment 4. According to recent studies (Ehn et al., 2014; Trostl et al., 2016; Mohr et al., 2017; McFiggans et al., 2019) dimers play an important role in new particle formation. Mohr et al. (2017) found decreased levels of gas-phase dimers in ambient air during NPF events, which is in line with our observations of lower dimer levels in the presence of particles in experiment 4, compared to experiment 3. A large enough concentration of low-volatility dimers obviously helps form critical nuclei that then grow by condensation. Note that the newly formed particles will provide an additional sink for dimers and thus reduce their presence as observable gas-phase products at the end of the flow reactor.

Influence of NO_x

In the experiments NOx1, $NOx3_H$, $NOx3_L$ and NOx9, the NO_x levels were increased (Table 1). As already described, NO_x was introduced to the Go:PAM as NO. After the addition of ozone, the ozone concentration decreases from 100 to $\sim$ 80 ppb in the experiment with lower NO_x levels and to $\sim$ 50 ppb in the experiment with higher NO_x levels, as it reacts with NO producing NO_2. For both high and low NO_x conditions, there is NO left after the initial reaction with ozone (see grey areas of Fig. S3). The presence of NO_x gave nitrogen-containing C_9 compounds with one or two N atoms and C_{18} compounds with only one N atom, in addition to HOM monomers and HOM dimers. These compounds are expected to be nitrates or peroxy nitrates, as it is highly unlikely to form nitro-aromatic compounds from TMB (Sato et al., 2012). N-containing compounds were the dominating species in experiments with NO_x (see Fig. 2), except for the experiment NOx1 with the smallest amount of NO_x added and a high OH exposure (NOx1). The amount of nitrated compounds increased with the amount of added NO_x at the expense of HOM monomers and HOM dimers as illustrated by the arrows in Fig. 2. The effect of the added NO_x is attenuated at higher OH exposure. For example, the nitrated monomers are reduced from 35.0 % and 38.9 % at low OH exposure down to 17.7 % and 30.2 % at high OH exposure. Under elevated NO_x conditions nitrated species were found among the 10 compounds with the highest contribution to the respective total signal (see the top-10 lists in Table S1 and Fig. 4).

For the two experiments with low OH exposure where the nitrated species dominated, 7 out of the top-10 species were nitrated with the highest signal arising from the di-nitrated compound ($C_9H_{14}N_2O_{10}$). In these two experiments the top-10 compounds contributed the most to the observed signal (42.3 % and 52.4 %), most likely owing to the high fraction of nitrated species acting as radical chain termination products. Under highest NO_x conditions, the high OH exposure experiment ($NOx3_H$) has 6 nitrated compounds in the top-

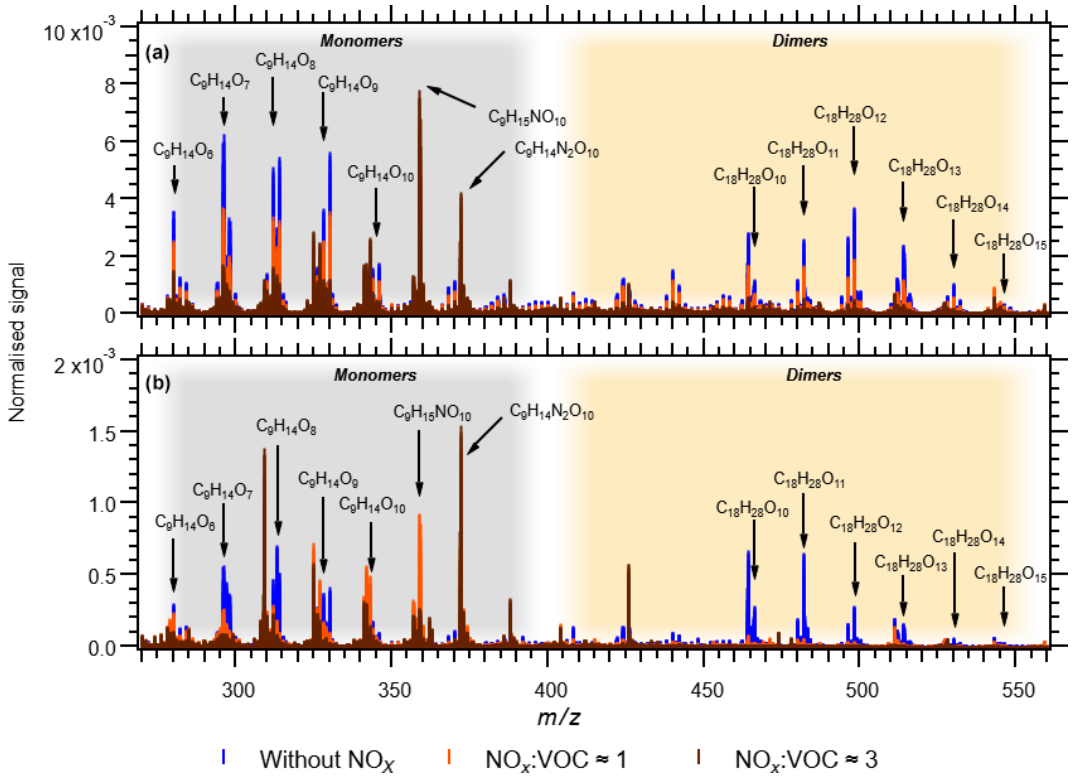

Figure 4. Comparison of mass spectra of HOM and nitrates. Panel **(a)** shows experiments 4 (blue), NOx1 (orange) and $NOx3_H$ (brown). Panel **(b)** shows experiments 2 (blue), $NOx3_L$ (orange) and NOx9 (brown).

10 list with the di-nitrated $C_9H_{14}N_2O_{10}$ on the second rank. In experiment NOx1 only 1 nitrated species ($C_9H_{15}NO_{10}$) is found in the top-10 list despite the elevated NO_x conditions.

Dimer formation is drastically reduced in the presence of elevated NO_x. The NO_x effect on NPF was clear and a high NO_x/ΔTMB ratio suppresses NPF from TMB oxidation, a trend that was also observed by Wildt et al. (2014) and Lehtipalo et al. (2018) for NPF from monoterpene oxidation. Whenever the products were dominated by ON ($NOx3_L$, NOx9 or $NOx3_H$) particle formation was not observed. Reduced particle formation was observed in NOx1 compared to experiment 1, which had a higher contribution of HOM. Owing to the importance of dimers for NPF, as reported by Lehtipalo et al. (2018), we suggest that the reaction of $RO_2 + NO$ resulting in ON is responsible for the observed reduced particle formation, because it competes with the dimer formation from $RO_2 + RO_2$. This reaction is also reducing the contribution of HOM monomers and dimers with increasing NO_x/ΔTMB ratio and decreasing OH exposure from a total of 61 % in exp NOx1 (OH exposure of 9.1×10^{10} molec s cm^{-3}) to 27.5 % in NOx9 (OH exposure of 6.3×10^9 molec s cm^{-3}). The reaction of $RO_2 + NO$ reduces the amount of HOM monomers and dimers, competing with autoxidation and termination by $RO_2 + RO_2$ or $RO_2 + HO_2$. The yield of ON from $NO + RO_2$ might be significant (e.g. up to 0.3) based on the measurable increase of ON and the decrease of NO_x in the system (Fig. S3).

The contribution of HOM monomer generations follows the general trend observed in experiments without NO_x. The first-generation HOMs have higher contribution at low OH exposures in $NOx3_L$ and NOx9, and the contribution of second-generation HOM is higher the higher the OH exposure is. Similarly, the contribution of $C_9H_{14}O_x$ is increasing with increasing OH exposure. Analogously to the families of HOM, different families of nitrates can be defined. Table 2 gives an overview of the nitrate families and how they contribute to the total signal in the experiments. At lowest OH exposures we find the highest contributions of first-generation nitrates ($C_9H_{13}NO_x$) as well as di-nitrates ($C_9H_{14}N_2O_x$). The contribution of second-generation nitrates ($C_9H_{15}NO_x$) is increasing with increasing OH exposure and is highest in $NOx3_H$.

For the formation of observed first-generation nitrates $C_9H_{13}NO_{6-12}$ ($C_9H_{13}NO_x$ in Table 2), we propose the reaction of a first-generation (HOM-)RO_2 with NO following the pathway

$$C_9H_{13}O_{5-11} + NO \rightarrow C_9H_{13}NO_{6-12}. \quad \text{(R11)}$$

The precursor $C_9H_{13}O_5$ is formed after one autoxidation step and its termination reaction with NO results in $C_9H_{13}NO_6$, which has only a minor contribution. $C_9H_{13}NO_7$

and $C_9H_{13}NO_8$, with higher contributions in exp $NOx3_L$ and NOx9, can be formed from the radicals $C_9H_{13}O_6$ and $C_9H_{13}O_7$, respectively. The even oxygen number in $C_9H_{13}O_6$ indicates that the compound should have undergone a transformation to RO (via reaction with RO_2 or NO) and subsequent H shift and further O_2 addition (Vereecken and Peeters, 2010; Mentel et al., 2015). A proposed detailed reaction mechanism is depicted in the Fig. 5.

Second-generation nitrates ($C_9H_{15}NO_{8-12}$) can be formed after an additional OH attack (and introduction of an additional H) on a first-generation (HOM) monomer, which explains the increase of these compounds with increasing OH exposure. The termination of the RO_2 radical chain with NO (Reaction R12) will then lead to the formation of the second-generation nitrate. The formation of RO_2 precursor species with 7–8 O numbers, i.e. $C_9H_{15}O_{7-8}$ likely stem from compounds terminated earlier in the radical chain process ($C_9H_{14}O_{4-5}$), which do not fall in the typical HOM class ($O:C \geq 6:9$). The reaction of a first-generation nitrate with OH, followed by autoxidation, could also possibly produce $C_9H_{15}NO_{8-12}$ by terminating via peroxy (Reaction R13) or hydroperoxy pathway (Reaction R14).

$$C_9H_{15}O_{7-11} + NO \rightarrow C_9H_{15}NO_{8-12}, \quad \text{(R12)}$$

$$C_9H_{14}NO_{9-13} + RO_2 \rightarrow C_9H_{15}NO_{8-12} + \text{Carbonyl products} + O_2, \quad \text{(R13)}$$

$$C_9H_{14}NO_{8-12} + HO_2 \rightarrow C_9H_{15}NO_{8-12} + O_2, \quad \text{(R14)}$$

For the formation of the most abundant di-nitrates of the formula $C_9H_{14}N_2O_{8-12}$ (Reaction R15), OH has to attack a nitrated compound $C_9H_{13}NO_{6-10}$ and the RO_2 radical chain has to be terminated with NO (Fig. 5).

$$C_9H_{14}NO_{7-11} + NO \rightarrow C_9H_{14}N_2O_{8-12} \quad \text{(R15)}$$

The precursor species $C_9H_{14}NO_7$ would be in this case formed from the OH attack on the smallest possible nitrate $C_9H_{13}NO_4$ (formed after one autoxidation step and NO termination).

It should be noted that the formation of peroxy nitrates via the reaction $RO_2 + NO_2 \rightarrow RO_2NO_2$ with alkyl and acyl-RO_2 (PAN-like, peroxyacyl nitrate) cannot be ruled out as a potential formation mechanism of nitrates.

The volatility of the produced ON seems to be too high (compared to dimers) to initiate NPF at the present concentrations as seen from the reduction in particle formation potential from experiment 4 (HOM dominated, particle formation) to NOx1 (reduction in HOM and increase in ON, reduced particle formation) and $NOx3_H$ (ON dominated, no particle formation).

Figure 2b shows the results for the evolution of HOM monomer, HOM dimers and organic nitrates (ONs) as calculated using the kinetic model described in detail in the Supplement. The model used has a very simplified scheme for TMB oxidation and subsequent RO_2 chemistry. We implemented a few rate coefficients suggested in the literature in order to demonstrate how those compare with our experimental results. Rate coefficients for RO_2 termination reactions from MCM in combination with rate coefficients of dimer formation by Berndt et al. (2018) (case 1 and 2 in Table S2) led to an overestimation of dimer compounds. Better representation of the observations was achieved by applying (a) the rate coefficients proposed by Zhao et al. (2018) for dimer formation (2.0×10^{-12} cm^3 molec^{-1} s^{-1}) and 1.0×10^{-12} cm^3 molec^{-1} s^{-1} for termination and RO formation with branching ratios of 0.4 and 0.6, respectively; (b) the rate coefficient (1.0×10^{-11} cm^3 molec^{-1} s^{-1}) from Berndt et al. (2018) for HOM-RO_2 + NO with a branching ratio of 0.3 for ON formation (Reaction R56 in Table S2)

In Fig. 2b, the calculated HOM dimer contribution is the sum of medium (produced from HOM-$RO_2 + RO_2$) and highly oxidised dimers (produced from HOM-RO_2 + HOM-RO_2), while the ONs include both organic nitrates (produced from HOM-RO_2 + NO) and peroxy nitrates (produced from HOM-$RO_2 + NO_2$). The increased production of monomers calculated for experiments 1 and 2 is in agreement with experimental results, where we observed a slightly larger contribution from monomers compared to dimers. Calculated concentrations for dimers are similar in experiment 3 and higher in experiment 4, compared to monomers. Secondary chemistry (reaction of OH with the products and possible formation of a second generation of HOM or nitrates) was not taken into consideration in the model. For the experiment with NO_x (Fig. 2b), the modelled product distribution follows the general trend of monomer, dimer and nitrate that we observe in the exp $NOx3_L$ and NOx9 with a general higher nitrate production compared to monomers and dimers. For the NO_x experiments with high initial ozone, the model can reproduce the higher HOM monomer and dimer levels in NOx1 but slightly overestimates the contribution of dimers. Particle formation was observed in NOx1, which might explain the overestimation owing to missing condensation sink in the model. Modelling $NOx3_H$ gives an overestimation of monomers and dimers.

In $NOx3_H$, modelled dimers start forming after $\sim$ 15 s. Almost all NO is converted to ON or NO_2 at this point, the reaction HOM-RO_2 + NO does not produce additional ON and the modelled levels of ON reach a plateau while the contribution of HOM dimers can increase. For experiments NOx1 and $NOx3_H$, the model is in better agreement with the measurements if only the HOM-dimer formation (from HOM-RO_2 + HOM-RO_2) is taken into account, i.e. highly oxidised dimers excluding medium oxidised dimer (from HOM-$RO_2 + RO_2$). Generally, the simplified model was able to support our analysis of the TMB chemistry as described above. Furthermore, it gave some support to the recently suggested mechanisms included in case 3 (e.g. Zhao et al., 2018).

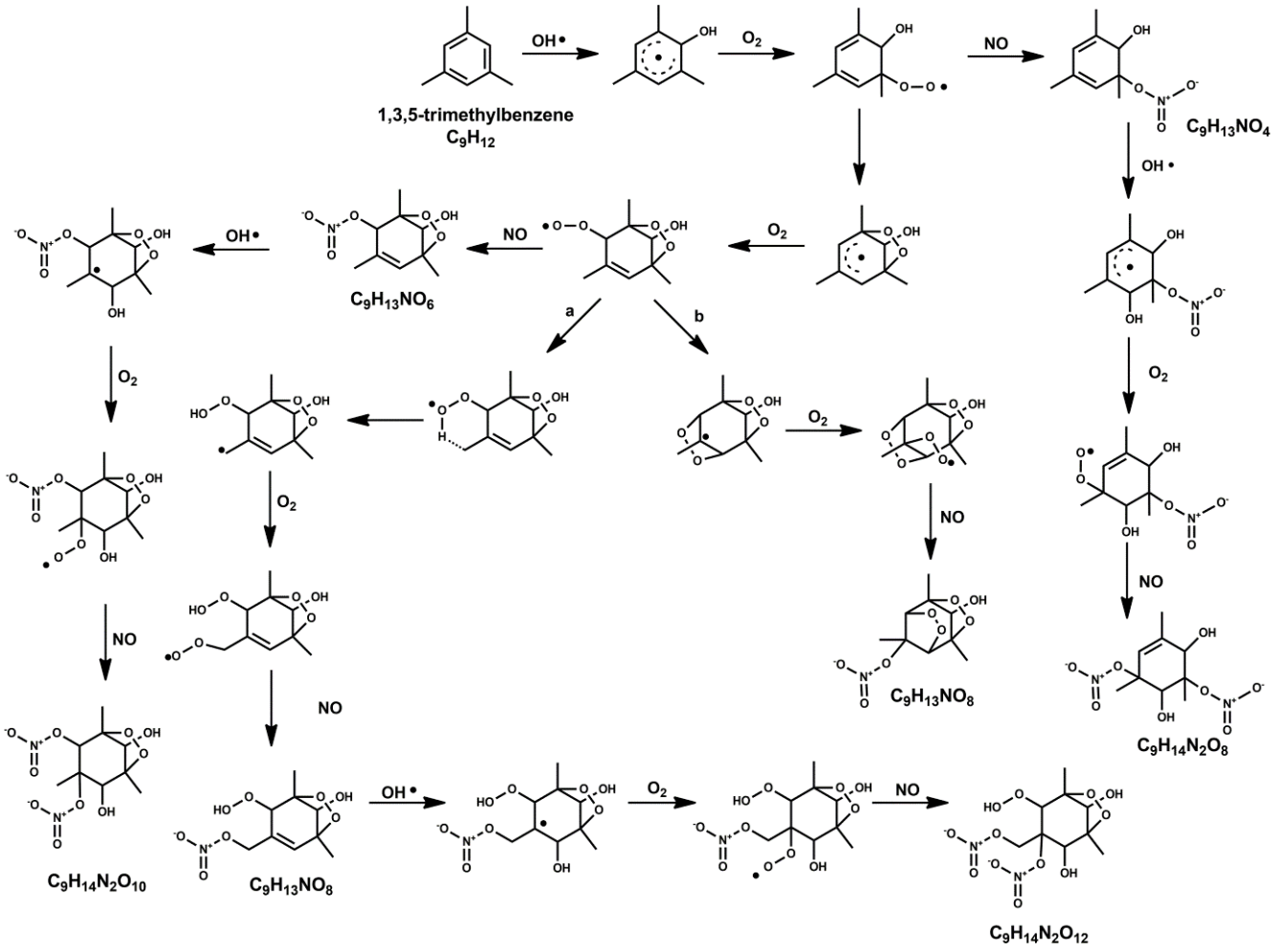

Figure 5. The proposed radical reaction mechanism for the formation of some of the mono- and di-nitrates from TMB mentioned in this study. Two separate mechanisms were suggested for the species with the formula $C_9H_{13}NO_8$, and formation pathways are based on **(a)** Wang et al. (2017) and **(b)** Molteni et al. (2018).

4 Atmospheric implication and conclusion

We have measured the formation of HOM monomers and dimers from OH-initiated oxidation of TMB. The experiments with highest OH exposures led to particle formation when NO_x was not added. With increasing OH exposure and increased likelihood of a second OH attack, we observe a higher contribution from second-generation oxidation products and dimers in general. The latter is attributed to the increased RO_2 concentrations from the increased and fast TMB consumption by OH. The observed products in this study match what would be expected as termination products from previously proposed reaction mechanisms for HOM formation.

The addition of NO_x to simulate urban conditions leads to the formation of ON in addition to HOM and a reduction in particle formation potential. We observe that the formation of ON is increasing with increasing NO_x/ΔTMB ratio, mostly at the expense of dimers. The presence of ONs, formed at the expense of dimers, can explain the decreased tendency for particle formation. We therefore suggest that the reaction of HOM-RO_2 + NO competes with the HOM-RO_2 self-reaction, yielding primarily a reduction in dimer formation, which is responsible for the reduction in particle formation. The experimental design using the Go:PAM with concentrations of HO_x (and RO_x) higher than ambient would attenuate the influence of added NO_x. This further emphasises the implication of our findings that most likely the NO_x effect would be even more important in the urban atmosphere.

According to studies by Molteni et al. (2018) and Wang et al. (2017), HOM formation from AVOCs was observed and consequently AVOC-HOM were suggested as potential contributors to observed NPF in urban atmospheres. In our study, under NO_x-free conditions, we found several previously identified HOMs even if we did not fully agree with the identity and relative importance of all HOMs. However,

the oxidation in polluted environments will happen under elevated NO_x levels and, as has been shown here, this can lead to the formation of ONs instead of HOMs and subsequently a reduction in NPF potential. We conclude that for interpretation of NPF from aromatics in urban areas, care should be taken and the OH exposure, NO_x levels and RO_2 concentrations need to be considered in detail since they will largely determine if the $HOM - RO_2 + NO$ can compete with reactions yielding HOM, and especially HOM dimers.

Data availability. The data set is available upon request by contacting Mattias Hallquist (hallq@chem.gu.se).

Supplement. The supplement related to this article is available online at: https://doi.org/10.5194/acp-19-15073-2019-supplement.

Author contributions. JH, ET, TFM and MH designed the experiments. JH and ET performed the experiments and data analysis. ET performed the modelling. CMS designed the chemical mechanisms. ET, JH and MH wrote the paper. All authors commented on the paper and were involved in the scientific interpretation and discussion.

Competing interests. The authors declare that they have no conflict of interest.

Acknowledgements. The research presented is a contribution to the Swedish strategic research area ModElling the Regional and Global Earth system, MERGE.

Financial support. This research has been supported by the Vetenskapsrådet (grant nos. 2014-05332 and 2013-06917) and the Svenska Forskningsrådet Formas (grant no. 2015-1537).

Review statement. This paper was edited by Manabu Shiraiwa and reviewed by two anonymous referees.

References

Atkinson, R., Baulch, D. L., Cox, R. A., Hampson, R. F., Kerr, J. A., and Troe, J.: Evaluated Kinetic and Photochemical Data for Atmospheric Chemistry Supplement-Iv - Iupac Subcommittee on Gas Kinetic Data Evaluation for Atmospheric Chemistry, J. Phys. Chem. Ref. Data, 21, 1125–1568, https://doi.org/10.1063/1.555918, 1992.

Berndt, T., Richters, S., Jokinen, T., Hyttinen, N., Kurten, T., Otkjaer, R. V., Kjaergaard, H. G., Stratmann, F., Herrmann, H., Sipila, M., Kulmala, M., and Ehn, M.: Hydroxyl radical-induced formation of highly oxidized organic compounds, Nat. Commun., 7, 13677, https://doi.org/10.1038/ncomms13677, 2016.

Berndt, T., Scholz, W., Mentler, B., Fischer, L., Herrmann, H., Kulmala, M., and Hansel, A.: Accretion product formation from self- and cross-reactions of RO_2 radicals in the atmosphere, Angew. Chemie, 57, 3820–3824, 2018.

Bianchi, F., Trostl, J., Junninen, H., Frege, C., Henne, S., Hoyle, C. R., Molteni, U., Herrmann, E., Adamov, A., Bukowiecki, N., Chen, X., Duplissy, J., Gysel, M., Hutterli, M., Kangasluoma, J., Kontkanen, J., Kurten, A., Manninen, H. E., Munch, S., Perakyla, O., Petaja, T., Rondo, L., Williamson, C., Weingartner, E., Curtius, J., Worsnop, D. R., Kulmala, M., Dommen, J., and Baltensperger, U.: New particle formation in the free troposphere: A question of chemistry and timing, Science, 352, 1109–1112, https://doi.org/10.1126/science.aad5456, 2016.

Bianchi, F., Garmash, O., He, X., Yan, C., Iyer, S., Rosendahl, I., Xu, Z., Rissanen, M. P., Riva, M., Taipale, R., Sarnela, N., Petäjä, T., Worsnop, D. R., Kulmala, M., Ehn, M., and Junninen, H.: The role of highly oxygenated molecules (HOMs) in determining the composition of ambient ions in the boreal forest, Atmos. Chem. Phys., 17, 13819–13831, https://doi.org/10.5194/acp-17-13819-2017, 2017.

Bianchi, F., Kurten, T., Riva, M., Mohr, C., Rissanen, M. P., Roldin, P., Berndt, T., Crounse, J. D., Wennberg, P. O., Mentel, T. F., Wildt, J., Junninen, H., Jokinen, T., Kulmala, M., Worsnop, D. R., Thornton, J. A., Donahue, N., Kjaergaard, H. G., and Ehn, M.: Highly Oxygenated Organic Molecules (HOM) from Gas-Phase Autoxidation Involving Peroxy Radicals: A Key Contributor to Atmospheric Aerosol, Chem. Rev., 119, 3472–3509, https://doi.org/10.1021/acs.chemrev.8b00395, 2019.

Chan, C. K. and Yao, X.: Air pollution in mega cities in China, Atmos. Environ., 42, 1–42, https://doi.org/10.1016/j.atmosenv.2007.09.003, 2008.

Crounse, J. D., Nielsen, L. B., Jorgensen, S., Kjaergaard, H. G., and Wennberg, P. O.: Autoxidation of Organic Compounds in the Atmosphere, J. Phys. Chem. Lett., 4, 3513–3520, https://doi.org/10.1021/jz4019207, 2013.

Donahue, N. M., Kroll, J. H., Pandis, S. N., and Robinson, A. L.: A two-dimensional volatility basis set – Part 2: Diagnostics of organic-aerosol evolution, Atmos. Chem. Phys., 12, 615–634, https://doi.org/10.5194/acp-12-615-2012, 2012.

Ehn, M., Kleist, E., Junninen, H., Petäjä, T., Lönn, G., Schobesberger, S., Dal Maso, M., Trimborn, A., Kulmala, M., Worsnop, D. R., Wahner, A., Wildt, J., and Mentel, T. F.: Gas phase formation of extremely oxidized pinene reaction products in chamber and ambient air, Atmos. Chem. Phys., 12, 5113–5127, https://doi.org/10.5194/acp-12-5113-2012, 2012.

Ehn, M., Thornton, J. A., Kleist, E., Sipila, M., Junninen, H., Pullinen, I., Springer, M., Rubach, F., Tillmann, R., Lee, B., Lopez-Hilfiker, F., Andres, S., Acir, I.-H., Rissanen, M., Jokinen, T., Schobesberger, S., Kangasluoma, J., Kontkanen, J., Nieminen, T., Kurten, T., Nielsen, L. B., Jorgensen, S., Kjaergaard, H. G., Canagaratna, M., Maso, M. D., Berndt, T., Petaja, T., Wahner, A., Kerminen, V.-M., Kulmala, M., Worsnop, D. R., Wildt, J., and Mentel, T. F.: A large source of low-volatility secondary organic aerosol, Nature, 506, 476–479, https://doi.org/10.1038/nature13032, 2014.

Eisele, F. L. and Tanner, D. J.: Measurement of the gas phase concentration of H_2SO_4 and methane sulfonic acid and estimates of

H_2SO_4 production and loss in the atmosphere, J. Geophys. Res.-Atmos., 98, 9001–9010, https://doi.org/10.1029/93jd00031, 1993.

Finlayson-Pitts, B. J. and Pitts, J. N.: Chemistry of the Upper and Lower Atmosphere: Theory, Experiments and Applications, Academic Press, San Diego, 2000.

Gentner, D. R., Jathar, S. H., Gordon, T. D., Bahreini, R., Day, D. A., El Haddad, I., Hayes, P. L., Pieber, S. M., Platt, S. M., de Gouw, J., Goldstein, A. H., Harley, R. A., Jimenez, J. L., Prevot, A. S. H., and Robinson, A. L.: Review of Urban Secondary Organic Aerosol Formation from Gasoline and Diesel Motor Vehicle Emissions, Environ. Sci. Technol., 51, 1074–1093, https://doi.org/10.1021/acs.est.6b04509, 2017.

Guo, S., Hu, M., Zamora, M. L., Peng, J., Shang, D., Zheng, J., Du, Z., Wu, Z., Shao, M., Zeng, L., Molina, M. J., and Zhang, R.: Elucidating severe urban haze formation in China, P. Natl. Acad. Sci. USA, 111, 17373–17378, https://doi.org/10.1073/pnas.1419604111, 2014.

Hallquist, M., Wenger, J. C., Baltensperger, U., Rudich, Y., Simpson, D., Claeys, M., Dommen, J., Donahue, N. M., George, C., Goldstein, A. H., Hamilton, J. F., Herrmann, H., Hoffmann, T., Iinuma, Y., Jang, M., Jenkin, M. E., Jimenez, J. L., Kiendler-Scharr, A., Maenhaut, W., McFiggans, G., Mentel, Th. F., Monod, A., Prévôt, A. S. H., Seinfeld, J. H., Surratt, J. D., Szmigielski, R., and Wildt, J.: The formation, properties and impact of secondary organic aerosol: current and emerging issues, Atmos. Chem. Phys., 9, 5155–5236, https://doi.org/10.5194/acp-9-5155-2009, 2009.

Hallquist, M., Munthe, J., Hu, M., Wang, T., Chan, C. K., Gao, J., Boman, J., Guo, S., Hallquist, A. M., Mellqvist, J., Moldanova, J., Pathak, R. K., Pettersson, J. B. C., Pleijel, H., Simpson, D., and Thynell, M.: Photochemical smog in China: scientific challenges and implications for air-quality policies, Nat. Sci. Rev., 3, 401–403, https://doi.org/10.1093/nsr/nww080, 2016.

Hu, M., Guo, S., Peng, J.-F., and Wu, Z.-J.: Insight into characteristics and sources of $PM_{2.5}$ in the Beijing–Tianjin–Hebei region, China, Nat. Sci. Rev., 2, 257–258, https://doi.org/10.1093/nsr/nwv003, 2015.

Huang, M., Lin, Y., Huang, X., Liu, X., Guo, X., Hu, C., Zhao, W., Gu, X., Fang, L., and Zhang, W.: Experimental study of particulate products for aging of 1,3,5-trimethylbenzene secondary organic aerosol, Atmos. Pollut. Res., 6, 209–219, https://doi.org/10.5094/apr.2015.025, 2015.

Intergovernmental Panel on Climate: Climate Change 2013 – The Physical Science Basis, Cambridge University Press, Cambridge, UK and New York, NY, USA, 1535 pp., 2014.

Jenkin, M. E., Saunders, S. M., Wagner, V., and Pilling, M. J.: Protocol for the development of the Master Chemical Mechanism, MCM v3 (Part B): tropospheric degradation of aromatic volatile organic compounds, Atmos. Chem. Phys., 3, 181–193, https://doi.org/10.5194/acp-3-181-2003, 2003.

Jokinen, T., Sipilä, M., Junninen, H., Ehn, M., Lönn, G., Hakala, J., Petäjä, T., Mauldin III, R. L., Kulmala, M., and Worsnop, D. R.: Atmospheric sulphuric acid and neutral cluster measurements using CI-APi-TOF, Atmos. Chem. Phys., 12, 4117–4125, https://doi.org/10.5194/acp-12-4117-2012, 2012.

Jokinen, T., Sipila, M., Richters, S., Kerminen, V. M., Paasonen, P., Stratmann, F., Worsnop, D., Kulmala, M., Ehn, M., Herrmann, H., and Berndt, T.: Rapid autoxidation forms highly oxidized RO_2 radicals in the atmosphere, Angewandte Chemie, 53, 14596–14600, https://doi.org/10.1002/anie.201408566, 2014.

Jokinen, T., Berndt, T., Makkonen, R., Kerminen, V. M., Junninen, H., Paasonen, P., Stratmann, F., Herrmann, H., Guenther, A. B., Worsnop, D. R., Kulmala, M., Ehn, M., and Sipila, M.: Production of extremely low volatile organic compounds from biogenic emissions: Measured yields and atmospheric implications, P. Natl. Acad. Sci. USA, 112, 7123–7128, https://doi.org/10.1073/pnas.1423977112, 2015.

Junninen, H., Ehn, M., Petäjä, T., Luosujärvi, L., Kotiaho, T., Kostiainen, R., Rohner, U., Gonin, M., Fuhrer, K., Kulmala, M., and Worsnop, D. R.: A high-resolution mass spectrometer to measure atmospheric ion composition, Atmos. Meas. Tech., 3, 1039–1053, https://doi.org/10.5194/amt-3-1039-2010, 2010.

Kang, E., Root, M. J., Toohey, D. W., and Brune, W. H.: Introducing the concept of Potential Aerosol Mass (PAM), Atmos. Chem. Phys., 7, 5727–5744, https://doi.org/10.5194/acp-7-5727-2007, 2007.

Kirkby, J., Duplissy, J., Sengupta, K., Frege, C., Gordon, H., Williamson, C., Heinritzi, M., Simon, M., Yan, C., Almeida, J., Trostl, J., Nieminen, T., Ortega, I. K., Wagner, R., Adamov, A., Amorim, A., Bernhammer, A. K., Bianchi, F., Breitenlechner, M., Brilke, S., Chen, X., Craven, J., Dias, A., Ehrhart, S., Flagan, R. C., Franchin, A., Fuchs, C., Guida, R., Hakala, J., Hoyle, C. R., Jokinen, T., Junninen, H., Kangasluoma, J., Kim, J., Krapf, M., Kurten, A., Laaksonen, A., Lehtipalo, K., Makhmutov, V., Mathot, S., Molteni, U., Onnela, A., Perakyla, O., Piel, F., Petaja, T., Praplan, A. P., Pringle, K., Rap, A., Richards, N. A., Riipinen, I., Rissanen, M. P., Rondo, L., Sarnela, N., Schobesberger, S., Scott, C. E., Seinfeld, J. H., Sipila, M., Steiner, G., Stozhkov, Y., Stratmann, F., Tome, A., Virtanen, A., Vogel, A. L., Wagner, A. C., Wagner, P. E., Weingartner, E., Wimmer, D., Winkler, P. M., Ye, P., Zhang, X., Hansel, A., Dommen, J., Donahue, N. M., Worsnop, D. R., Baltensperger, U., Kulmala, M., Carslaw, K. S., and Curtius, J.: Ion-induced nucleation of pure biogenic particles, Nature, 533, 521–526, https://doi.org/10.1038/nature17953, 2016.

Kristensen, K., Watne, Å. K., Hammes, J., Lutz, A., Petäjä, T., Hallquist, M., Bilde, M., and Glasius, M.: High-Molecular Weight Dimer Esters Are Major Products in Aerosols from α-Pinene Ozonolysis and the Boreal Forest, Environ. Sci. Technol. Lett., 3, 280–285, https://doi.org/10.1021/acs.estlett.6b00152, 2016.

Kurtén, T., Tiusanen, K., Roldin, P., Rissanen, M., Luy, J.-N., Boy, M., Ehn, M., and Donahue, N.: α-Pinene Autoxidation Products May Not Have Extremely Low Saturation Vapor Pressures Despite High O : C Ratios, J. Phys. Chem. A, 120, 2569–2582, https://doi.org/10.1021/acs.jpca.6b02196, 2016.

Lee, B. H., Mohr, C., Lopez-Hilfiker, F. D., Lutz, A., Hallquist, M., Lee, L., Romer, P., Cohen, R. C., Iyer, S., Kurtén, T., Hu, W., Day, D. A., Campuzano-Jost, P., Jimenez, J. L., Xu, L., Ng, N. L., Guo, H., Weber, R. J., Wild, R. J., Brown, S. S., Koss, A., de Gouw, J., Olson, K., Goldstein, A. H., Seco, R., Kim, S., McAvey, K., Shepson, P. B., Starn, T., Baumann, K., Edgerton, E. S., Liu, J., Shilling, J. E., Miller, D. O., Brune, W., Schobesberger, S., D'Ambro, E. L., and Thornton, J. A.: Highly functionalized organic nitrates in the southeast United States: Contribution to secondary organic aerosol and reactive nitrogen budgets, P. Natl. Acad. Sci. USA, 113, 1516–1521, https://doi.org/10.1073/pnas.1508108113, 2016.

Lehtipalo, K., Yan, C., Dada, L., Bianchi, F. Xiao, M., Wagner, R., Stolzenburg, D., Ahonen, L. R., Amorim, A., Baccarini, A., Bauer, P. S., Baumgartner, B., Bergen, A., Bernhammer, A.-K., Breitenlechner, M., Brilke, S., Buchholz, A., Buenrostro Mazon, S., Chen, D., Chen, X., Dias, A., Dommen, J., Draper, D. C., Duplissy, J., Ehn, M., Finkenzeller, H., Fischer, L., Frege, C.,Fucks, C., Garmash, O., Gordon, H., Hakala, J., He, X., Heikkinen, L., Heinritzi, M., Helm, J. C., Hofbauer, V., Hoyle, C. R., Jokinen, T., Kangasluoma, J., Kerminen, V.-M., Kim, C., Kirkby, J., Kontkanen, J., Kürten, A., Lawler, M. J., Mai, H., Mathot, S., Mauldin III, R. L., Molteni, U., Nichman, L., Nie, W., Nieminen, T., Ojdanic, A., Onnela, A., Passananti, M., Petäjä, T., Piel, F., Pospisilova, V., Quéléver, L. L. J., Rissanen, M. P., Rose, C., Sarnela, N., Schallhart, S., Schuchmann, S., Sengupta, K., Simon, M., Sipilä, M., Tauber, C., Tomé, A., Tröstl, J., Väisänen, O., Vogel, A. L., Volkamer, R., Wagner, A. C., Wang, M., Weitz, L., Wimmer, D., Ye, P., Ylisirniö, A., Zha, Q., Carslaw, K. S., Curtius, J., Donahue, N. M., Flagan, R. C., Hansel, A., Riipinen, I., Virtanen, A., Winkler, P. M., Baltensperger, U., Kulmala, M., and Worsnop, D. R.: Multicomponent new particle formation acid, ammonia, and biogenic vapors, Sci. Adv., 4, eaau5363, https://doi.org/10.1126/sciadv.aau5363, 2018.

McFiggans, G., Mentel, T. F., Wildt, J., Pullinen, I., Kang, S., Kleist, E., Schmitt, S., Springer, M., Tillmann, R., Wu, C., Zhao, D., Hallquist, M., Faxon, C., Le Breton, M., Hallquist, A. M., Simpson, D., Bergstrom, R., Jenkin, M. E., Ehn, M., Thornton, J. A., Alfarra, M. R., Bannan, T. J., Percival, C. J., Priestley, M., Topping, D., and Kiendler-Scharr, A.: Secondary organic aerosol reduced by mixture of atmospheric vapours, Nature, 565, 587–593, https://doi.org/10.1038/s41586-018-0871-y, 2019.

McGraw, R. and Zhang, R.: Multivariate analysis of homogeneous nucleation rate measurements. Nucleation in the p-toluic acid/sulfuric acid/water system, J. Chem. Phys., 128, 064508, https://doi.org/10.1063/1.2830030, 2008.

Mentel, T. F., Springer, M., Ehn, M., Kleist, E., Pullinen, I., Kurtén, T., Rissanen, M., Wahner, A., and Wildt, J.: Formation of highly oxidized multifunctional compounds: autoxidation of peroxy radicals formed in the ozonolysis of alkenes – deduced from structure–product relationships, Atmos. Chem. Phys., 15, 6745–6765, https://doi.org/10.5194/acp-15-6745-2015, 2015.

Mohr, C., Lopez-Hilfiker, F. D., Yli-Juuti, T., Heitto, A., Lutz, A., Hallquist, M., D'Ambro, E. L., Rissanen, M. P., Hao, L. Q., Schobesberger, S., Kulmala, M., Mauldin, R. L., Makkonen, U., Sipila, M., Petaja, T., and Thornton, J. A.: Ambient observations of dimers from terpene oxidation in the gas phase: Implications for new particle formation and growth, Geophys. Res. Lett., 44, 2958–2966, https://doi.org/10.1002/2017gl072718, 2017.

Molteni, U., Bianchi, F., Klein, F., El Haddad, I., Frege, C., Rossi, M. J., Dommen, J., and Baltensperger, U.: Formation of highly oxygenated organic molecules from aromatic compounds, Atmos. Chem. Phys., 18, 1909–1921, https://doi.org/10.5194/acp-18-1909-2018, 2018.

Paulsen, D., Dommen, J., Kalberer, M., Prevot, A. S., Richter, R., Sax, M., Steinbacher, M., Weingartner, E., and Baltensperger, U.: Secondary organic aerosol formation by irradiation of 1,3,5-trimethylbenzene-NO_x-H_2O in a new reaction chamber for atmospheric chemistry and physics, Environ. Sci. Technol., 39, 2668–2678, https://doi.org/10.1021/es0489137, 2005.

Rissanen, M. P., T. Kurtén, M. Sipilä, J. A. Thornton, J. Kangasluoma, N. Sarnela, H. Junninen, S. Jørgensen, S. Schallhart, M. K. Kajos, R. Taipale, M. Springer, T. F. Mentel, T. Ruuskanen, T. Petäjä, D. R. Worsnop, H. G. Kjaergaard, and M. Ehn: The formation of highly oxidized multifunctional products in the ozonolysis of cyclohexene, J. Am. Chem. Soc., 136, 44, 15596–15606, 2014.

Rodigast, M., Mutzel, A., and Herrmann, H.: A quantification method for heat-decomposable methylglyoxal oligomers and its application on 1,3,5-trimethylbenzene SOA, Atmos. Chem. Phys., 17, 3929–3943, https://doi.org/10.5194/acp-17-3929-2017, 2017.

Sato, K., Takami, A., Kato, Y., Seta, T., Fujitani, Y., Hikida, T., Shimono, A., and Imamura, T.: AMS and LC/MS analyses of SOA from the photooxidation of benzene and 1,3,5-trimethylbenzene in the presence of NO_x: effects of chemical structure on SOA aging, Atmos. Chem. Phys., 12, 4667–4682, https://doi.org/10.5194/acp-12-4667-2012, 2012.

Shrivastava, M., Cappa, C. D., Fan, J. W., Goldstein, A. H., Guenther, A. B., Jimenez, J. L., Kuang, C., Laskin, A., Martin, S. T., Ng, N. L., Petaja, T., Pierce, J. R., Rasch, P. J., Roldin, P., Seinfeld, J. H., Shilling, J., Smith, J. N., Thornton, J. A., Volkamer, R., Wang, J., Worsnop, D. R., Zaveri, R. A., Zelenyuk, A., and Zhang, Q.: Recent advances in understanding secondary organic aerosol: Implications for global climate forcing, Rev. Geophys., 55, 509–559, https://doi.org/10.1002/2016rg000540, 2017.

Trostl, J., Chuang, W. K., Gordon, H., Heinritzi, M., Yan, C., Molteni, U., Ahlm, L., Frege, C., Bianchi, F., Wagner, R., Simon, M., Lehtipalo, K., Williamson, C., Craven, J. S., Duplissy, J., Adamov, A., Almeida, J., Bernhammer, A. K., Breitenlechner, M., Brilke, S., Dias, A., Ehrhart, S., Flagan, R. C., Franchin, A., Fuchs, C., Guida, R., Gysel, M., Hansel, A., Hoyle, C. R., Jokinen, T., Junninen, H., Kangasluoma, J., Keskinen, H., Kim, J., Krapf, M., Kurten, A., Laaksonen, A., Lawler, M., Leiminger, M., Mathot, S., Mohler, O., Nieminen, T., Onnela, A., Petaja, T., Piel, F. M., Miettinen, P., Rissanen, M. P., Rondo, L., Sarnela, N., Schobesberger, S., Sengupta, K., Sipilaa, M., Smith, J. N., Steiner, G., Tome, A., Virtanen, A., Wagner, A. C., Weingartner, E., Wimmer, D., Winkler, P. M., Ye, P. L., Carslaw, K. S., Curtius, J., Dommen, J., Kirkby, J., Kulmala, M., Riipinen, I., Worsnop, D. R., Donahue, N. M., and Baltensperger, U.: The role of low-volatility organic compounds in initial particle growth in the atmosphere, Nature, 533, 527–531, https://doi.org/10.1038/nature18271, 2016.

Vereecken, L. and Peeters, J.: A structure–activity relationship for the rate coefficient of H-migration in substituted alkoxy radicals, 12, 12608–12620, https://doi.org/10.1039/C0CP00387E, 2010.

Wang, S., Wu, R., Berndt, T., Ehn, M., and Wang, L.: Formation of Highly Oxidized Radicals and Multifunctional Products from the Atmospheric Oxidation of Alkylbenzenes, Environ. Sci. Technol., 51, 8442–8449, https://doi.org/10.1021/acs.est.7b02374, 2017.

Watne, Å. K., Psichoudaki, M., Ljungström, E., Le Breton, M., Hallquist, M., Jerksjö, M., Fallgren, H., Jutterström, S., and Hallquist, Å. M.: Fresh and Oxidized Emissions from In-Use Transit Buses Running on Diesel, Biodiesel, and CNG, Environ. Sci. Technol., 52, 7720–7728, https://doi.org/10.1021/acs.est.8b01394, 2018.

WHO: Ambient air pollution: A global assessment of exposure and burden of disease, World Health Organ., 1–131, 2016.

Wildt, J., Mentel, T. F., Kiendler-Scharr, A., Hoffmann, T., Andres, S., Ehn, M., Kleist, E., Müsgen, P., Rohrer, F., Rudich, Y., Springer, M., Tillmann, R., and Wahner, A.: Suppression of new particle formation from monoterpene oxidation by NO_x, Atmos. Chem. Phys., 14, 2789–2804, https://doi.org/10.5194/acp-14-2789-2014, 2014.

Wyche, K. P., Monks, P. S., Ellis, A. M., Cordell, R. L., Parker, A. E., Whyte, C., Metzger, A., Dommen, J., Duplissy, J., Prevot, A. S. H., Baltensperger, U., Rickard, A. R., and Wulfert, F.: Gas phase precursors to anthropogenic secondary organic aerosol: detailed observations of 1,3,5-trimethylbenzene photooxidation, Atmos. Chem. Phys., 9, 635–665, https://doi.org/10.5194/acp-9-635-2009, 2009.

Yan, C., Nie, W., Äijälä, M., Rissanen, M. P., Canagaratna, M. R., Massoli, P., Junninen, H., Jokinen, T., Sarnela, N., Häme, S. A. K., Schobesberger, S., Canonaco, F., Yao, L., Prévôt, A. S. H., Petäjä, T., Kulmala, M., Sipilä, M., Worsnop, D. R., and Ehn, M.: Source characterization of highly oxidized multifunctional compounds in a boreal forest environment using positive matrix factorization, Atmos. Chem. Phys., 16, 12715–12731, https://doi.org/10.5194/acp-16-12715-2016, 2016.

Zhao, Y., Thornton, J. A., and Pye, H. O. T.: Quantitative constraints on autoxidation and dimer formation from direct probing of monoterpene-derived peroxy radical chemistry, P. Natl. Acad. Sci. USA, 115, 12142–12147, https://doi.org/10.1073/pnas.1812147115, 2018.